PAUL SCHERRER INSTITUT

PSI

Memorandum

Datum: September 10, 2009

Von: Andreas Suter
Telefon: 42 38
Raum: WLGA / 119
e-mail: andreas.suter@psi.ch

An:

cc:

Analysis of the Nonlocal Effects in In-37, Beam Time June 09

In the following sections I am going to describe the analysis performed on the In-37 sample. I will not reproduce any nonlocal theory formulae which can be found in A. Suter *et al.*, PRB**72**, 024506 (2005). I will start the discussion with the time domain analysis.

Time Domain Analysis

The μ^+ spin polarization is modelled by the following components:

$$P_{\rm P}(t) = \int_0^d n(z)\, \cos(\gamma_\mu B(z) t) dz, \tag{1}$$

where d is the film thickness, $n(z)$ is the μ^+ stopping distribution (see Fig.8), and $B(z)$ is

$$B(z) = \begin{cases} B_{\rm ext} & : \quad z < z_0 \text{ or } z > d - z_0, \\ B_{\rm P}(z - z_0) & : \quad z \geq z_0 \text{ and } z \leq d - z_0 \end{cases}, \tag{2}$$

where z_0 is the dead layer thickness, and $B_{\rm P}(z - z_0)$ is the Pippard-Meissner screening field profile[1]. For the temperature dependence of λ, the two fluid model one is chosen, i.e. $\lambda(T/T_c) \propto 1/\sqrt{1-(T/T_c)^4}$, and for $\xi_{\rm P}(T/T_c)$ see the above reference Eq.(6). For the fits $\xi_{\rm P}(0) = \xi_0$ was kept constant to $\xi_0 = 380$nm.

The full μ^+ spin polarization is than given by:

$$P_\mu(t) = w \cdot P_{\rm P}(t) \exp\left[-1/2(\sigma_{\rm s} t)^2\right] + (1-w) \exp\left[-1/2(\sigma_{\rm Bkg} t)^2\right] \cos(\gamma_\mu B_{\rm ext} t), \tag{3}$$

where w is the weight of the signal from the sample, and $\sigma_{\rm s}$ is an additional broadening we always need to account for the data. The second term describes the background due to μ^+ stopping in the sample plate, shield, etc. Typically $1 - w \approx 0.1 - 0.15$. That this approach accounts well for the data is shown in Fig.1.

Here I will shortly discuss the results which are collected in Figs.2–4.

Asymmetries: The sample asymmetries (see Fig.2) show smaller values at lower implantation energies. This is an expected feature due to μ^+ back-scattering, though I didn't try to quantify it yet. The maximum asymmetry for the LEM instrument is about 0.28. Taking the sum of the sample and background signal this is about what is found.

London penetration depth $\lambda_{\rm L}$: If the described modell would be perfectly catching the experimental situation, the fitted $\lambda_{\rm L}$'s should be nothing than a constant (for all energies and temperatures). This is obviously not the case as seen in Fig.3. There are 2 obvious reasons

[1] in case the film thickness d is small, $B_{\rm P}(z)$ will be calculate as a proper superposition of a penetrating field from both sides.

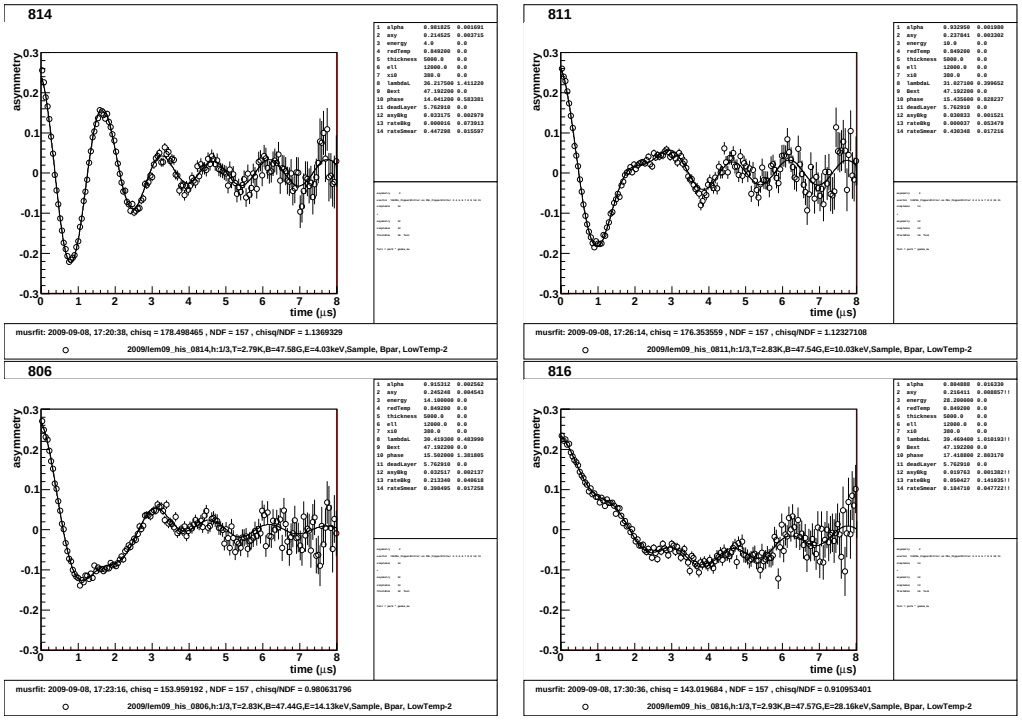

Figure 1: All spectra for $T = 2.83$K ($T_c = 3.415$K). Top left: $E = 4.0$keV, top right: $E = 10.0$keV, bottom left: $E = 14.1$keV, bottom right: $E = 28.2$keV

for the observed energy and temperature dependence: (i) the modell assumes that the order parameter is constant up to the very surface. This is unlikely to be the case (see also the discussion of the Ta data in the above PRB). This could indeed be the reason why an increase of $\lambda_{\rm L}$ is found at low implantation energies. (ii) the temperature dependence of $\lambda_{\rm L}$ is likely to be caused by deviations from the two-fluid approximation as well as the previously stated point. Still, it is interesting to note that the observed trend for In is opposite to our previous findings on Pb (PRB Fig.9).

It is a pity that lower temperature are not yet available since $\lambda_{\rm L}$ will saturate at some point. For the moment the best value is the one obtained at the lowest temperature, i.e. $\lambda_{\rm L} = 29.9(1)$nm (obtained from a global fit at $T = 2.83$K).

Dead Layer thickness d : The dead layer values were obtained from the global fits at each temperature. The values are given in Tab.1.

T (K)	z_0 (nm)
2.83	5.8(1)
3.0	3.5(3)
3.1	4.6(1)

Table 1: Dead layer values found from global fits at each temperature.

Depolarization rates: Fig.4 shows the found depolarization rates. The background rates $\sigma_{\rm Bkg}$ are small as expected ($\sigma_{\rm Bkg} \lesssim 0.1\ \mu{\rm sec}^{-1}$). However it was necessary to add an additional broadening to the Pippard polarization function $P_{\rm P}(t)$ (see Eq.(1)) as given in Eq.(3). This we find in all superconductors we studied so far (low-T_c's and high-T_c's). It seems that $\sigma_{\rm s}$ is tracking the magnetization of the superconductor, but we do not quite understand this effect yet. There are various ideas around: dipole fields due to sample roughness, locally trapped flux due to sample misalignment (i.e. magnetic axis is not parallel to the sample surface), etc.

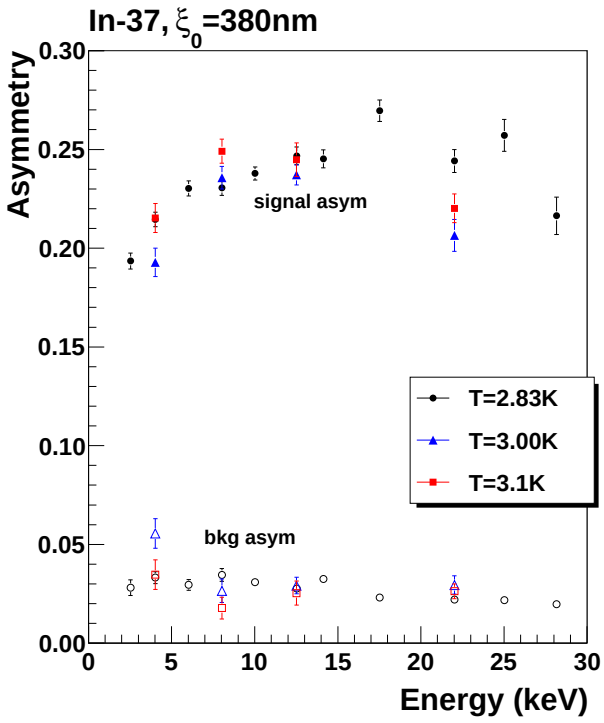

Figure 2: Asymmetries obtained of fits according the described modell.

Nonlocal magnetic Meissner profile $B(z)$

During the online analysis we have approximated $P_{\rm P}(t)$ by the following Gaussian approximation $P_{\rm G}(t)$:

$$P_{\rm G}(t) = \exp\left[-1/2(\sigma_{\rm G}t)^2\right]\cos(\gamma B_{\rm G}t). \tag{4}$$

The obtained values for $B_{\rm G}$ plotted against $\langle z\rangle$ obtained from the stopping distribution are shown in Figs.5-7. As can be seen the $B(z)$ dependency is deviating from the exponential behavior as expected for nonlocal electro-magnetic response. In order to get a more realistic representation of the data, the following approach was used: for each temperature a global fit to all energies was performed with $\lambda_{\rm L}$, z_0, and the detector phase as global parameter, and fixing the externally applied field to the value obtained from $T > T_c$, using the modell from Eq.(3). In the next step all the fits were repeated for individual energies/temperature by just fixing z_0 to the value found from the global fit. This was necessary since z_0 and $\lambda_{\rm L}$ are highly correlated for single energy fits but not for global fits. The parameters found this way are shown in Figs.2-4 (see also Tabs.2-4). In order to give a representation of $B(z)$ the mean value $\langle B\rangle$ for the stated parameters was calculated:

$$\langle B\rangle = \int_0^\infty B(z)\, n(z)\, dz \,/\, \int_0^\infty n(z)dz \tag{5}$$

$\langle B\rangle$ versus $\langle z\rangle$ is shown in Figs.5-7. As can be seen, the $B_{\rm G}$ suggests a slightly shorter $\lambda_{\rm L}$. The solid curve shown in Figs..5-7 are the nonlocal $B(z)$'s according to the values from the global fit, i.e. it is *not* a fit to the data points!

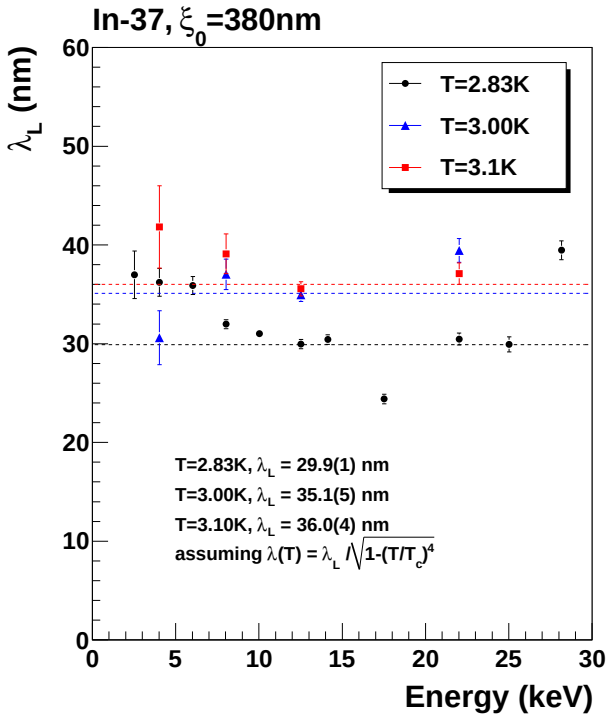

Figure 3: Extracted London penetration depths λ_L. The lines show the values obtained from a global fit (color coded as the points from single fits), and these global fit values are given explicitly in the figure.

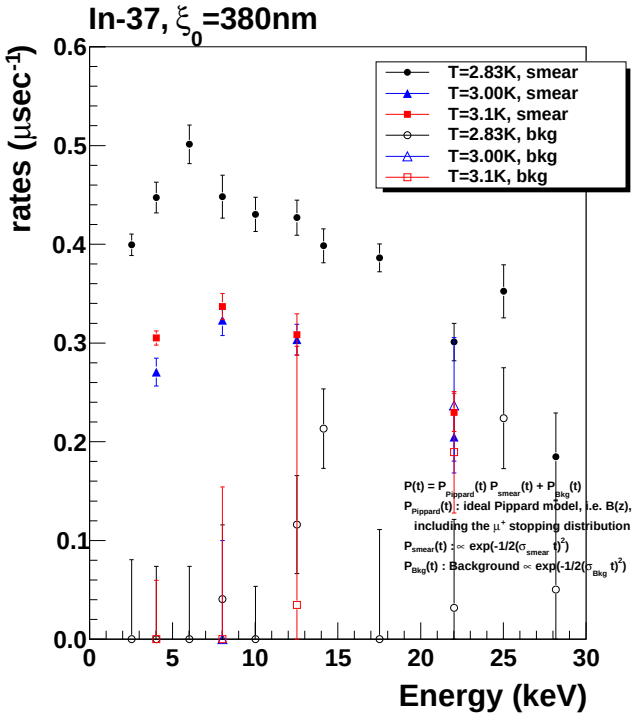

Figure 4: Extracted depolarization rates according to Eq.(3).

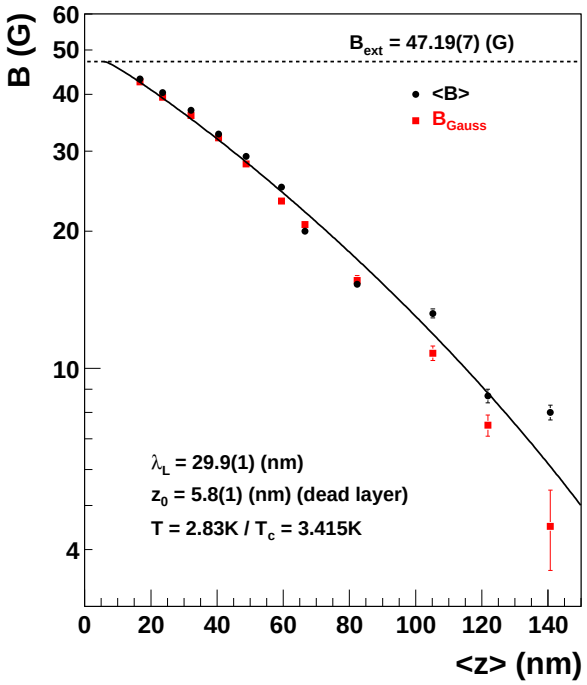

Figure 5: Nonlocal magnetic Meissner screening profile $B(z)$ at $T = 2.83$K. Black bullets: $\langle B \rangle$ according to Eq.(5). Red squares: screened field estimate according to a Gaussian fit (see the text and Eq.(4)). Black curve: nonlocal screening profile according to the global time domain fit. It is *not* a fit of the data points. The dashed line shows the external field value.

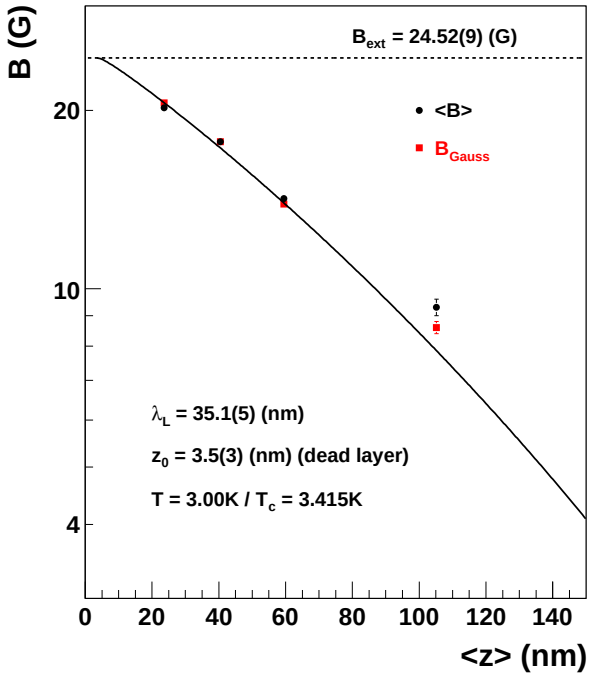

Figure 6: Nonlocal magnetic Meissner screening profile $B(z)$ at $T = 3.00$K. Black bullets: $\langle B \rangle$ according to Eq.(5). Red squares: screened field estimate according to a Gaussian fit (see the text and Eq.(4)). Black curve: nonlocal screening profile according to the global time domain fit. It is *not* a fit of the data points. The dashed line shows the external field value.

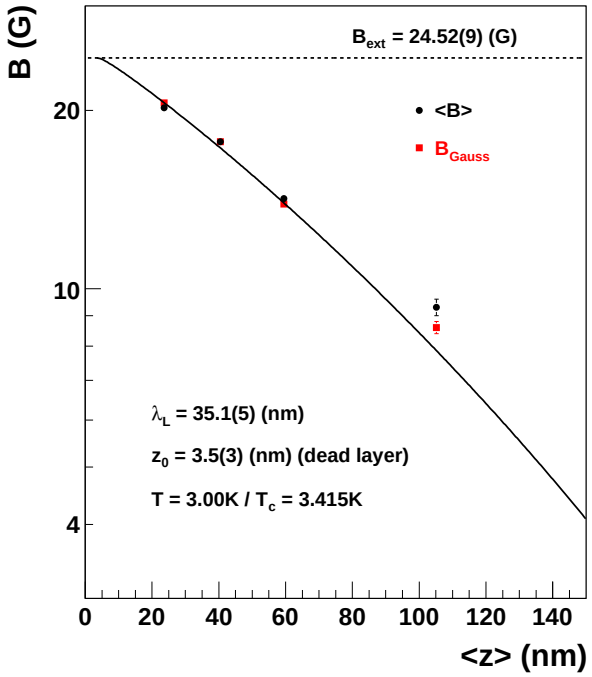

Figure 7: Nonlocal magnetic Meissner screening profile $B(z)$ at $T = 3.10$K. Black bullets: $\langle B \rangle$ according to Eq.(5). Red squares: screened field estimate according to a Gaussian fit (see the text and Eq.(4)). Black curve: nonlocal screening profile according to the global time domain fit. It is *not* a fit of the data points. The dashed line shows the external field value.

μ^+ stopping distribution in In and Sn

Fig.8 shows the μ^+ stopping distribution $n(z)$ as calculated by `trim.sp`.

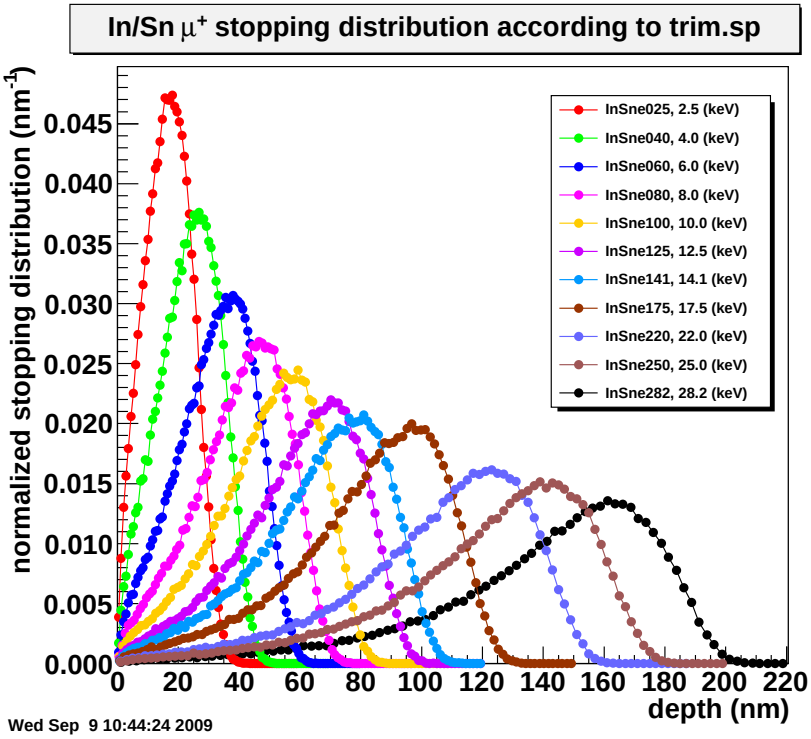

Figure 8: μ^+ stopping distribution in In and Sn calculated with `trim.sp`.

Fitting results as tables

run	E (keV)	λ_L (nm)	$\langle z \rangle$ (nm)	$\langle B \rangle$ (G)	B_G (G)	$\lambda = 1/B_{ext} \int B(z)dz$ (nm)
806	14.1	30.4(5)	66.6	20.0(2)	20.7(3)	65.5
807	25.0	29.9(8)	121.8	8.7(3)	7.5(4)	64.6
808	22.0	30.5(6)	105.3	13.2(3)	10.8(4)	65.7
809	17.5	24.4(5)	82.3	15.3(3)	15.6(4)	55.2
810	12.5	29.9(5)	59.5	25.0(3)	23.3(3)	64.6
811	10.0	31.0(4)	48.8	29.2(2)	28.1(2)	66.6
812	8.0	32.0(4)	40.5	32.7(2)	32.1(2)	68.3
813	6.0	35.9(8)	32.1	36.9(2)	35.9(2)	75.2
814	4.0	36.2(1.2)	23.6	40.3(1)	39.4(4)	75.7
815	2.5	37.0(2.0)	16.7	43.2(2)	42.6(4)	77.1
816	28.2	39.5(1.0)	140.7	8.0(3)	4.5(9)	81.4

Table 2: $B_{ext} = 47.19(7)$G, $T = 2.83$K, $z_0 = 5.76$nm, $\langle B \rangle$ see Eq.(5) and the text, B_G see Eq.(4) and the text. From the global fit: $\lambda_L = 29.9(1)$nm

run	E (keV)	λ_L (nm)	$\langle z \rangle$ (nm)	$\langle B \rangle$ (G)	B_G (G)	$\lambda = 1/B_{ext} \int B(z)dz$ (nm)
822	4.0	30.6(2.9)	23.6	20.2(3)	20.6(3)	70.8
823	8.0	37.0(1.4)	40.5	17.7(3)	17.7(2)	83.0
824	12.5	34.9(7)	59.5	14.2(1)	13.9(1)	79.0
825	22.0	39.4(1.3)	105.3	9.3(3)	8.6(2)	87.5

Table 3: $B_{ext} = 24.52(9)$G, $T = 3.00$K, $z_0 = 3.5$nm, $\langle B \rangle$ see Eq.(5) and the text, B_G see Eq.(4) and the text. From the global fit: $\lambda_L = 35.1(5)$nm

run	E (keV)	λ_L (nm)	$\langle z \rangle$ (nm)	$\langle B \rangle$ (G)	B_G (G)	$\lambda = 1/B_{ext} \int B(z)dz$ (nm)
826	22.0	37.1(1.1)	105.3	9.8(3)	9.4(2)	91.7
827	12.5	35.6(7)	59.5	15.2(1)	14.9(1)	88.6
828	8.0	39.1(2.0)	40.5	18.6(3)	18.5(3)	95.5
829	4.0	41.8(4.0)	23.6	21.6(2)	21.2(6)	101.1

Table 4: $B_{ext} = 24.52(9)$G, $T = 3.10$K, $z_0 = 4.59$nm, $\langle B \rangle$ see Eq.(5) and the text, B_G see Eq.(4) and the text. From the global fit: $\lambda_L = 36.0(4)$nm